Towards Open-Set Fault Diagnosis for Reactor Coolant Pumps under Unknown Fault Conditions

Jonghyeok Kim[1], Jeongmin Oh[2], Jueun Lee[3], Minseok Choi[4], and Hyunseok Oh[5]

[1,2,3,4,5] *Department of Mechanical and Robotics Engineering, Gwangju Institute of Science and Technology, Gwangju, 61005, Republic of Korea*

enfycius@gm.gist.ac.kr
jmoh1010@gm.gist.ac.kr
ljcish26@gm.gist.ac.kr
mschoi1104@gm.gist.ac.kr
hsoh@gist.ac.kr

ABSTRACT

The reactor coolant pump – vibration monitoring system (RCP-VMS) ensures the safe operation of nuclear power plants by detecting anomalies in the shaft and bearing components of reactor coolant pumps. While effective for known fault modes, conventional Artificial Intelligence (AI)-based diagnostic models often fail to detect unseen faults, especially when labeled data are limited. To address this limitation, an open-set recognition approach based on class-specific semantic reconstruction (CSSR), referred to as vibration displacement image CSSR (VDI-CSSR) in this study, is proposed. Vibration signals collected from RCP-VMS are processed into orbit plot and recurrence plots, which serve as multi-channel image inputs to the model. The reconstruction errors are then used to distinguish both known and unknown fault conditions. Experimental results demonstrate that the proposed method achieves competitive closed-set accuracy while significantly enhancing open-set fault detection performance compared to baseline models. This approach enhances the reliability and robustness of fault diagnosis in safety-critical rotating machinery such as RCPs.

1. INTRODUCTION

The reactor coolant pump – vibration monitoring system (RCP-VMS) plays a vital role in ensuring the safe and stable operation of nuclear power plants. It continuously monitors the dynamic behavior of the RCP by analyzing vibration signals acquired from accelerometers and non-contact displacement sensors. The signals are used to detect early signs of shaft misalignment, bearing defects, and other mechanical anomalies (Choi et al., 2025; Hwang et al., 2025; Choi et al., 2025). While RCP-VMS is effective at identifying known fault conditions, real-world applications often involve a wide variety of fault modes, including previously unseen or evolving faults. Conventional artificial intelligence (AI) models for fault diagnosis typically rely on supervised learning, which require extensive labeled datasets and tend to perform poorly when encountering novel conditions outside the scope of the training data (Hu et al., 2025). This limitation becomes especially critical in safety-critical systems like RCPs. Collecting and labeling fault data in nuclear environments is extremely challenging, making it difficult to ensure sufficient coverage of all possible fault scenarios. Li et al. (2024) proposed an OSR framework for nuclear power plant fault diagnosis based on convolutional prototype learning (CPL). This approach enhanced inter-class separability and intra-class compactness, demonstrating higher discriminative power than conventional CNNs and improving unknown fault detection performance. However, CPL does not incorporate semantic reconstruction during training, and therefore cannot fully capture the latent semantic structure of high-dimensional, nonlinear industrial data. To address these challenges, this paper proposes an open-set recognition (OSR) framework based on class-specific semantic reconstruction (CSSR) for robust fault diagnosis in RCP-VMS. Huang et al. (2022) proposed CSSR, which integrates class-specific feature extraction with semantic reconstruction. This approach complements the limitations of CPL and enables the learning of richer semantic representations, thereby allowing more effective discrimination of unknown fault conditions. In the proposed method, vibration signals are converted into multi-channel image representations—including orbit plot and recurrence plots (RPs)—which are used as input to the diagnostic model. The reconstruction error is then leveraged to differentiate between known and unknown fault modes. Through both the simulation study and the RK4 journal bearing testbed data, it was demonstrated that the proposed method not only achieves competitive closed-set classification accuracy, but also significantly improves the detection of unseen fault conditions, enhancing both the reliability and robustness of RCP-VMS.

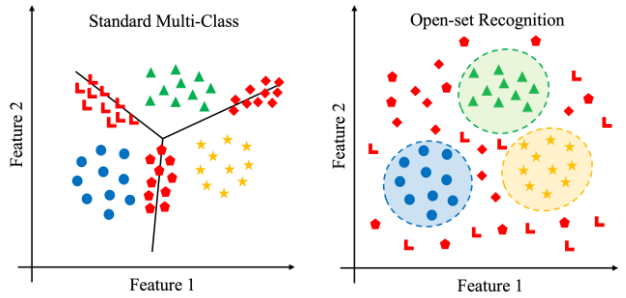

(a) (b)

Figure 1. Transition from closed-set classification to open-set recognition: (a) standard multi-class classification without unknown awareness; (b) open-set recognition with unknown rejection capability.

2. THEORETICAL BACKGROUND

Most classifiers assume a closed-set environment defined during the training phase, classifying every input at test time as belonging to one of the previously learned classes. However, in real-world scenarios, unknown classes that were not used during training may appear, and in such cases, closed-set classifiers inevitably assign them to one of the known classes. As discussed earlier, OSR can address this issue. OSR rejects inputs from classes not included in the training set, thereby preventing incorrect predictions. Scheirer et al. (2013) defined the notion of open space risk to formalize this problem.

Conventional deep learning models utilize a softmax layer at the final stage to normalize class scores into probabilities, which leads to the limitation of assigning high probabilities to specific classes even for unknown classes. To address this issue, Bendale and Boult (2015) proposed OpenMax, which computes the distance between the input and class distributions using the activation vector (AV) and mean activation vector (MAV), and estimates the outlier probability through a Weibull distribution based on extreme value theory.

Recently, Huang et al. (2022) proposed CSSR, which has attracted considerable attention. CSSR employs class-specific autoencoders (AEs) to reconstruct semantic features and computes class membership probabilities based on reconstruction errors. This approach mitigates the issues of excessive distributional compression and boundary blurring in conventional methods, while enhancing class-related representations by reconstructing semantic features from the backbone network rather than raw pixels. The reconstruction error is defined as follows:

$$d(\boldsymbol{z}, A_c) = \| \boldsymbol{z} - A_c(\boldsymbol{z}) \|_1 \approx \max_{\boldsymbol{v} \in V_c} \| \boldsymbol{z} - \boldsymbol{v} \|_1 \qquad (1)$$

where z denotes the latent representation of an input sample x extracted via the encoder, $A_c(\cdot)$ represents the class-specific autoencoder corresponding to class c, and V_c denotes the set of prototypes (representative vectors) for class c. This measures the distance between a data point and the class-specific manifold, thereby quantifying the otherness of the sample with respect to that manifold. Under the assumption that smaller errors indicate a higher likelihood of belonging to that class, the error is directly used as the classification logit. The equation for computing the class membership probability is expressed as follows:

$$p(\boldsymbol{y} = \boldsymbol{i} | \boldsymbol{z}, \boldsymbol{A}) = \frac{\exp(-\gamma \cdot d(\boldsymbol{z}, A_i))}{\sum_{j=1}^{m} \exp(-\gamma \cdot d(\boldsymbol{z}, A_i))} \qquad (2)$$

where m denotes the total number of classes, and γ is a hyperparameter that controls the sharpness or discriminative strength of the probability distribution. A larger γ value amplifies the effect of small differences in reconstruction error on the probability values, resulting in a sharper, more class-discriminative probability distribution. In this approach, the autoencoder is trained to minimize the reconstruction error for data belonging to its corresponding class, while being encouraged to remain sufficiently distant from other class manifolds. The reconstruction error is measured using the mean absolute error (MAE) as the default metric. As training progresses, the known classes exhibit enhanced relevant features, whereas unknown classes generally show low feature activations.

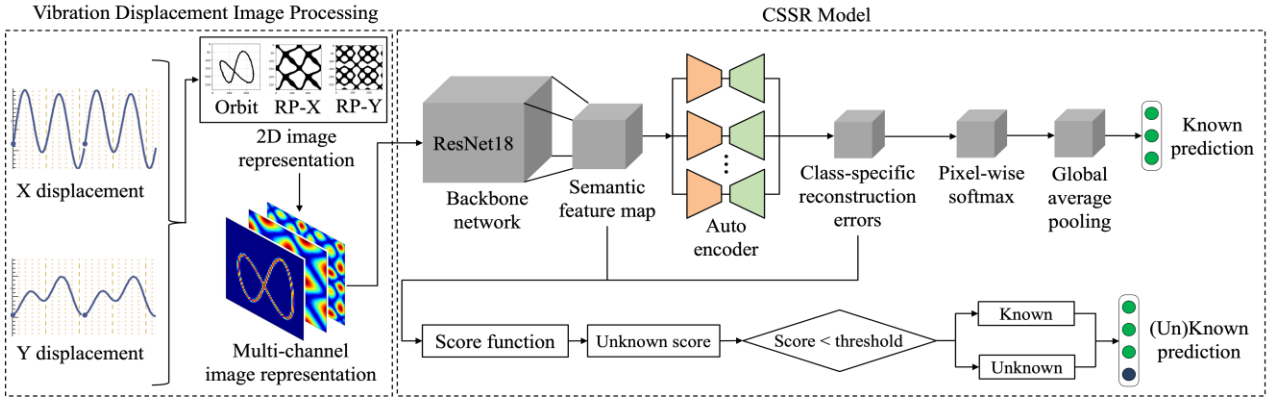

Figure 2. Overview of the proposed method.

3. PROPOSED METHOD

The proposed method, referred to as VDI-CSSR, consists of two stages including vibration displacement image processing and the CSSR model, as depicted in Fig. 2.

3.1. Vibration Displacement Image Processing

Fault signal data from the RCP-VMS operating in the field are difficult to collect, and their distribution tends to be highly imbalanced. To address this issue, this study utilized synthesized two-axis (*X, Y*) vibration displacement signals generated through physics-based simulation (Lee et al., 2025). In addition, the RK4 journal bearing dataset acquired from the GE Bently Nevada testbed (Jeon et al., 2015) was also utilized. The simulation data were produced using a model that incorporates the geometric characteristics and operating conditions of the rotor, as well as empirical physical knowledge. The RK4 dataset was collected under real experimental conditions, reflecting various practical factors such as sensor noise, environmental variations, and signal distortion. Compared to the simulation dataset, these characteristics provide a more realistic representation of field conditions, making RK4 an important reference for evaluating the practicality and robustness of the proposed method. In addition, both the simulation data and the RK4 data were acquired at the same sampling rate of 8,500 Hz, and the same image conversion procedure was applied to both time-series datasets.

The time-domain signals were transformed into two-dimensional patterns such as orbit plot and RPs. Specifically, for the two-axis vibration displacement signals $x(t)$ and $y(t)$ acquired over the same time interval, the complex trajectory was defined as $D(t) = x(t) + jy(t)$, and the orbit plot was generated by visualizing its temporal evolution. In addition, for each axis, the recurrence matrix was computed as $R_{ij} = \Theta(\varepsilon - ||x(t_i) - x(t_j)||)$, and these matrices were used to generate the RP-X and RP-Y images. This conversion process projects the temporal dependencies and structural variations of the original time-domain signals into two-dimensional patterns, enabling the dynamic characteristics of vibration to be more effectively utilized as model inputs.

An orbit plot represents the phase relationship between vibration displacements in the *X* and *Y* directions, illustrating changes in the shape of the vibration trajectory according to rotor conditions such as unbalance, eccentricity, and misalignment. For example, a perfectly circular orbit plot indicates a balanced state, whereas an elliptical or distorted orbit plot suggests unbalance or structural defects. An RP visualizes the recurrence patterns of a time series in its state-space trajectory, revealing the periodicity, quasi-periodicity, nonstationarity, and nonlinear dynamical characteristics of the system (Eckmann et al., 1987). In an RP, distinct dot patterns and diagonal structures reflect the periodic behavior of normal operation, while irregular dot distributions indicate aperiodic behavior caused by faults or disturbances.

The generated images are resampled to the same resolution (64×64) and normalized to the range [0, 1], then combined along the channel dimension to form a single 3-channel input tensor. This step, instead of using the raw signals directly, transforms the geometric and dynamic structures of the vibration signals into image patterns, enabling the model to capture fault indications more effectively through time-feature-based learning.

3.2. CSSR Model

The CSSR architecture is adopted and combined with vibration displacement image processing to form the proposed VDI-CSSR method for vibration-based fault detection in an open-set environment. CSSR employs a dedicated autoencoder for each class, which reconstructs the semantic features of that class. This design naturally leads to low reconstruction errors for known classes and high reconstruction errors for unknown or different classes. Such a property aligns with the operational principle of the RCP-VMS, which must make conservative rejection decisions for unknown inputs. In particular, CSSR offers several advantages: (1) it can maintain closed-set classification accuracy while also achieving strong unknown-class detection performance, (2) it allows direct formulation of a rejection criterion based on reconstruction error without requiring an additional anomaly detection module, and (3) it internalizes the semantic structure of each class, enabling effective discrimination of complex fault patterns. For these reasons, we determined that CSSR is a highly suitable model architecture for the multi-axis vibration data-based open-set fault detection problem addressed in this study.

The generated input images are fed into a shared backbone encoder (i.e., ResNet-18) to produce latent representations (He et al., 2016). The orbit plot and RPs visually encode, respectively, the geometric trajectory changes of rotating machinery motion and the time-delay correlation structure. Under normal conditions, these representations form stable and repetitive patterns for each class. The backbone encoder extracts the shape, density, and periodicity of these patterns and maps them into class-specific distributions in a low-dimensional latent space. This latent representation branches into two pathways: (1) one leading to a softmax classification head for identifying known classes, and (2) another directed to a set of class-specific decoders for reconstructing the input images. During training, classification and reconstruction are jointly optimized. For normal classes, the corresponding class-specific autoencoder learns to accurately reconstruct fine-grained details in the orbit plot and RP patterns (e.g., orbital curvature, RP dot distribution). In contrast, for inputs from unknown or different classes, a margin constraint is applied so that the reconstruction quality by the corresponding class decoder degrades sharply, thereby

reinforcing class boundaries. Through this process, CSSR internalizes the dynamic characteristics embedded in the orbit plot and RPs as class-dependent reconstructability.

During inference, the reconstruction error for each class is computed, and the class with the smallest error is provisionally selected as the predicted class. At the same time, the maximum softmax probability from the classification head is obtained. For normal inputs, the learned orbit plot and RP patterns from training match well, resulting in both low reconstruction error and high classification probability. In contrast, unknown inputs show high reconstruction errors across all decoders due to pattern mismatches, and their classification probabilities are also low. Both values are standardized in advance using the validation set and then combined with equal weighting to form a single unknown score. If this score is smaller than the predefined threshold, the input is accepted as "known" for the predicted class; if it is greater, the input is rejected as "unknown".

4. EXPERIMENTAL SETUP

The simulation dataset was constructed such that only known classes were used during the training phase. Specifically, as shown in Table 1, the training set consisted of four known classes: normal (NO), forced unbalance (FU), heavy preload (HP), and mild preload (MP). For the validation set, two additional classes—angular misalignment (AM) and oil whirl (OW)—were designated as unknown classes. For the test set, three different classes—combined misalignment (CM), oil whirl + heavy unbalance (OH), and oil whirl + mild unbalance (OM)—were used as unknowns to evaluate performance in the open-set scenario. As summarized in Table 1, the training split contained a total of 800 samples from the four known classes. The validation split included 2,000 samples in total, consisting of the known classes plus AM and OW as unknowns. Likewise, the test split contained 2,000 samples in total, with CM, OH, and OM serving as unknown classes not present in training.

The RK4 dataset used three known classes (normal, unbalance, and misalignment) for training, as shown in Table 2. The validation set additionally included Oil whirl as an unknown class, while the test set used Rubbing as another unknown class to evaluate generalization performance. The training set contained a total of 450 samples from the three known classes, and both the validation and test sets consisted of 800 samples each, containing a mixture of the known classes and their corresponding unknown classes. By intentionally keeping the unknown class combinations in the test set disjoint from those in the validation set, the reliability of the performance evaluation was enhanced. Accordingly, in both the simulation dataset and the RK4 dataset, only a minimal amount of labeled training data was intentionally used to simulate the data-scarce conditions commonly encountered in real industrial environments.

Table 1. Configuration for the simulation dataset.

Split	Classes	Total samples
Train	NO, FU, HP, MP	800
Validation	NO, FU, HP, MP + Unknown (AM, OW)	2,000
Test	NO, FU, HP, MP + Unknown (CM, OH, OM)	2,000

Table 2. Configuration for the RK4 dataset.

Split	Classes	Total samples
Train	NO, UB, MA	450
Validation	NO, UB, MA + Unknown (OW)	800
Test	NO, UB, MA + Unknown (RB)	800

All dataset splits were constructed without sample overlap, and threshold/hyperparameter selection was conducted using the validation dataset. For a fair comparison with the proposed method, all models were implemented using the same backbone network (ResNet-18), and the input layer of each method was modified to match the channel dimension of the input images. All methods were trained for 100 epochs, and the results after 100 epochs were used for comparison. Each class-specific autoencoder in the CSSR architecture was configured with hidden dimensions of [128, 64, 32] to enhance reconstruction performance. Stochastic gradient descent (SGD) was used as the optimizer. To minimize the loss of physical meaning, no data augmentation techniques were employed. Model selection during training was based primarily on minimizing the loss. The checkpoint corresponding to the minimum validation loss was stored as the final model, and its performance was evaluated on the test set containing a disjoint set of unseen fault modes, demonstrating that the model did not overfit to the limited validation unknown classes. For comparison, softmax thresholding and OpenMax were adopted as baseline methods. Softmax thresholding rejects an input as unknown if its maximum softmax probability falls below the threshold, with the threshold range explored from 0.5 to 0.95 (Table 2). OpenMax computes the class-specific MAV and distance distribution, fits a Weibull distribution to each class tail, and recalibrates/redistributes logits accordingly. The Weibull tail size was explored in the range of 20–400, alpha in the range of 1–min (10, number of classes), and the unknown rejection threshold in the range of 0.6–0.99 (Table 3). Hyperparameter search was performed using Optuna to maximize open-set detection accuracy on the validation split.

Table 3. Hyperparameter search space.

Method	Hyperparameter	Search Range
Softmax thresholding	Softmax threshold	0.5 to 0.95
OpenMax	Weibull tail	20 to 400
	Weibull alpha	1 to 10
	Weibull threshold	0.6 to 0.99

5. RESULTS

5.1. Simulation Datasets

The proposed method was evaluated under two input configurations: orbit plot only and orbit plot with RPs. Using Optuna, hyperparameters were searched within the parameter ranges specified in Table 3 based on model accuracy, and the resulting optimal hyperparameters are summarized in Table 4. Table 5 reports the mean accuracy and standard deviation obtained from five independent training runs. When using orbit plots only as input, CSSR achieved average validation and test accuracies of 82.8±0.015% and 85.6±0.032%, respectively. In comparison, OpenMax obtained 67.4±0.024% and 67.8±0.024% for validation and test, while Softmax thresholding achieved 77.9±0.007% and 76.6±0.021%, respectively. In other words, CSSR consistently showed superior performance to both baseline methods. In contrast, when orbit plots were combined with recurrence plots, CSSR achieved average validation and test accuracies of 96.9±0.040% and 99.7±0.004%, respectively. Based on the test dataset, adding recurrence plots improved the performance of CSSR by approximately 14.1% and improved OpenMax by approximately 23.8%, whereas Softmax thresholding slightly decreased by about 0.5%. In addition, as shown in Figure 3, the misclassification of unknown classes observed when using orbit plots alone was largely mitigated when both orbit and recurrence plots were used together.

Table 4. Hyperparameter settings.

Inputs	Methods	Hyperparameter	Value
Orbit	Softmax thresholding	Softmax threshold	0.76
	OpenMax	Weibull tail	101
		Weibull alpha	4
		Weibull threshold	0.65
	CSSR	Autoencoder latent	64
Orbit and RPs	Softmax thresholding	Softmax threshold	0.55
	OpenMax	Weibull tail	23
		Weibull alpha	2
		Weibull threshold	0.68
	CSSR (Proposed)	Autoencoder latent	64

Table 5. Fault diagnostic performance.

Inputs	Methods	Accuracy (Validation/test) (%)	Standard deviation (Validation/test) (%)
Orbit	Softmax thresholding	77.9/76.6	**0.007**/**0.021**
	OpenMax	67.4/67.8	0.024/0.024
	CSSR	**82.8**/**85.6**	0.015/0.032
Orbit and RPs	Softmax	72.9/76.1	**0.007**/0.006
	OpenMax	89.3/91.6	0.015/0.012
	CSSR (Proposed)	**96.9**/**99.7**	0.040/**0.004**

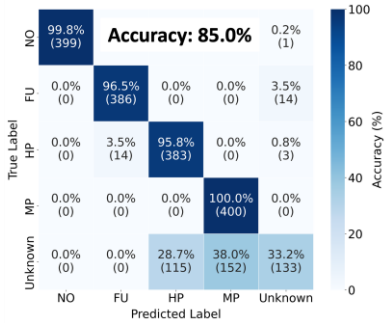

(a)

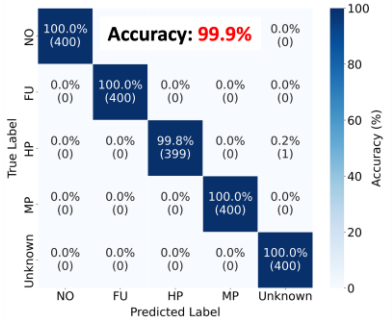

(b)

Figure 3. Performance improvement of CSSR with (a) orbit plot only and (b) orbit plot with RPs.

5.2. RK4 Datasets

Performance on the RK4 dataset was examined using the same two input configurations to evaluate whether the benefit of incorporating recurrence plots is consistently observed under real testbed conditions. The optimal hyperparameters were determined based on validation accuracy as shown in Table 6, and the final performance was obtained by averaging the results over five independent runs as summarized in Table 7. When using orbit plots only, CSSR achieved average validation and test accuracies of 96.6±0.003% and 97.1±0.030%, respectively. In comparison, OpenMax obtained 92.2±0.010% for both validation and test, and Softmax thresholding obtained 75.0±0.000% and 86.4±0.034% for validation and test, respectively. When recurrence plots were additionally included, CSSR achieved average validation and test accuracies of 96.6±0.005% and 99.0±0.012%, respectively. Based on the test dataset, adding recurrence plots improved the performance of OpenMax by approximately 4.8% and improved CSSR by approximately 1.9%, whereas Softmax thresholding decreased by approximately 6.5%. Furthermore, as shown in Figure 4, the orbit-only configuration caused a degradation in the known-class performance due to the influence of unknown classes, whereas such degradation did not occur when both plots were jointly considered.

Table 6. Hyperparameter settings.

Inputs	Methods	Hyperparameter	Value
Orbit	Softmax thresholding	Softmax threshold	0.72
	OpenMax	Weibull tail	83
		Weibull alpha	3
		Weibull threshold	0.81
	CSSR	Autoencoder latent	32
Orbit and RPs	Softmax thresholding	Softmax threshold	0.61
	OpenMax	Weibull tail	20
		Weibull alpha	3
		Weibull threshold	0.79
	CSSR (Proposed)	Autoencoder latent	32

Table 7. Fault diagnostic performance.

Inputs	Methods	Accuracy (Validation/test) (%)	Standard deviation (Validation/test) (%)
Orbit	Softmax thresholding	75.0/86.4	**0.000**/0.034
	OpenMax	92.2/92.2	0.010/**0.010**
	CSSR	**96.6/97.1**	0.003/0.030
Orbit and RPs	Softmax	75.0/79.9	**0.000**/0.042
	OpenMax	**97.0**/97.0	0.008/**0.008**
	CSSR (Proposed)	96.6/**99.0**	0.005/0.012

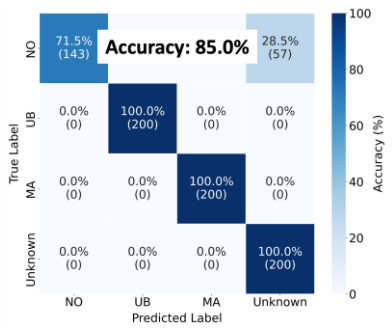

(a)

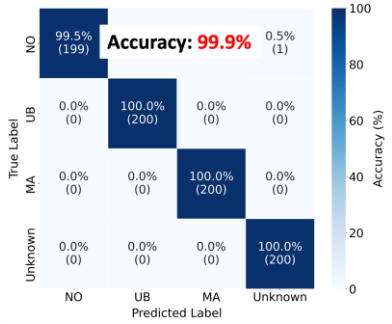

(b)

Figure 4. Performance improvement of CSSR with (a) orbit plot only and (b) orbit plot with RPs.

6. Conclusion

The proposed VDI-CSSR method was validated using both a simulation-based dataset and the RK4 journal bearing experimental dataset. Only a limited number of samples were intentionally used during training, and different combinations of unknown classes were assigned to the validation and test datasets to minimize the possibility of overfitting. Nevertheless, the model selected based on the validation dataset consistently showed strong performance on the test dataset, indicating that the proposed approach can generalize effectively even under limited-label conditions. Furthermore, the CSSR-based approach maintained closed-set classification accuracy while achieving significantly superior rejection capability for unknown faults compared to Softmax thresholding and OpenMax. In particular, the multi-channel input configuration that combines orbit plots with recurrence plots contributed to consistently improving open-set recognition performance compared to using orbit plots alone. These results demonstrate that the proposed VDI-CSSR method can effectively learn meaningful features even in data-constrained scenarios, and has high potential for generalization in safety-critical industrial environments where reliability and robustness are required.

This study does not cover conditions that may occur in actual nuclear power plant environments. Future work will incorporate a practical diagnostic procedure that reflects real operational scenarios, applying a step-wise open-set diagnosis structure in which normal/abnormal discrimination is performed first, followed by detailed fault mode identification. In addition, the design of unknown classes will be redefined to focus on fault modes with higher diagnostic value than impeller unbalance, such as oil whirl, oil whip, and shaft-related defects. Real order-tracked data acquired during the cost-down period will also be utilized to perform validation at a field-deployable level. Based on this, DC components and order-based features will be incorporated into the diagnostic process, and domain adaptation techniques will be integrated to reduce dependence on labeled data and further improve unknown fault detection performance.

Acknowledgment

This work was supported by the National Research Foundation of Korea (NRF) grant funded by the Korea government (MSIT) (No. RS-2022-00144441, No. RS-2025-00517566), by the Korea Institute for Advancement of Technology (KIAT) grant funded by the Korea government (MOTIE) (No. RS-2025-02263945, HRD Program for Industrial Innovation), and by the InnoCORE program of the Ministry of Science and ICT(N10250154).

REFERENCES

Choi, J., Oh, J., Ko, T., Chung, B., Choi, Y.-C., Lee, S., & Oh, H. (2025). Intelligent metallic loose part monitoring in three-dimensional structures using convolutional neural networks and the position-invariant loss function. *Nuclear Engineering and Technology*, 57(7), 103474. https://doi.org/10.1016/j.net.2025.103474.

Hwang, M., Choi, M., & Oh, H. (2025). Frequency-enhanced neural networks with a hybrid spall-size estimator for bearing fault diagnosis. *Journal of Computational Design and Engineering*, 12(5), 1–20. https://doi.org/10.1093/jcde/qwaf040.

Choi, M., Lee, C., Park, S., Hwang, M., & Oh, H. (2025). Frequency-enhanced network with self-supervised learning for anomaly detection of hydraulic piston pumps. *Expert Systems with Applications*, 282, 127662. https://doi.org/10.1016/j.eswa.2025.127662.

Hu, M., Luo, C., Wang, C., & Qiang, Z. (2025). Compound fault recognition and diagnosis of rolling bearing in open-set-recognition setting. *Measurement*, 242 (Part D), 116132. https://doi.org/10.1016/j.measurement.2024.116132.

Li, J., Lin, M., Wang, B., Tian, R., Tan, S., Li, Y., & Chen, J. (2024). Open set recognition fault diagnosis framework based on convolutional prototype learning network for nuclear power plants. *Energy*, 290, 130101. https://doi.org/10.1016/j.energy.2023.130101.

Scheirer, W. J., de Rezende Rocha, A., Sapkota, A., & Boult, T. E. (2013). Toward open set recognition. *IEEE Transactions on Pattern Analysis and Machine Intelligence*, 35(7), 1757–1772. https://doi.org/10.1109/TPAMI.2012.256.

Bendale, A., & Boult, T. E. (2016). Towards open set deep networks. *Proceedings of the IEEE Conference on Computer Vision and Pattern Recognition* (*CVPR*), 1563–1572. https://doi.org/10.1109/CVPR.2016.173.

Huang, H., Wang, Y., Hu, Q., & Cheng, M. M. (2022). Class-specific semantic reconstruction for open set recognition. *IEEE transactions on pattern analysis and machine intelligence*, 45(4), 4214-4228.

Lee, D., Lee, J. G., Choi, M., Park, C., Kim, C. W., Niu, G., & Oh, H. (2025). Multi-fidelity sub-label-guided transfer network with physically interpretable synthetic datasets for rotor fault diagnosis. *Engineering Applications of Artificial Intelligence*, 148, 110467. https://doi.org/10.1016/j.engappai.2025.110467.

Jeon, B. C., Jung, J. H., & Youn, B. D. (2015). Datum unit optimization for robustness of a journal bearing diagnosis system. *International Journal of Precision Engineering and Manufacturing*, 16(12), 2411–2425. https://doi.org/10.1007/s12541-015-0311-y.

Eckmann, J.-P., Kamphorst, S. O., & Ruelle, D. (1987). Recurrence plots of dynamical systems. *Europhysics Letters*, 4(9), 973. https://doi.org/10.1209/0295-5075/4/9/004.

He, K., Zhang, X., Ren, S., & Sun, J. (2016). Deep residual learning for image recognition. In *Proceedings of the IEEE conference on computer vision and pattern recognition* (pp. 770-778).

BIOGRAPHIES

Jonghyeok Kim received the B.S. degree in civil and environmental engineering from Hanbat National University, Daejeon, Republic of Korea, in 2024, where he is currently pursuing the M.S. degree in mechanical and robotics engineering from Gwangju Institute of Science and Technology, Gwangju, Republic of Korea. His current research interest includes prognostics and health management for RCP-VMS.

Jeongmin Oh received the B.S. degree in mechanical design engineering from Pukyong National University, Busan, Republic of Korea, in 2022, the M.S. degree in mechanical engineering from the Gwangju Institute of Science and Technology, Gwangju, Republic of Korea, in 2024, where he is currently pursuing the Ph.D. degree in mechanical and robotics engineering from Gwangju Institute of Science and Technology, Gwangju, Republic of Korea. His current research interest includes prognostics and health management for RCP-VMS.

Jueun Lee received the B.S. degree in mechanical engineering from Pukyong National University, Busan, Republic of Korea, in 2024, where she is currently pursuing the M.S. degree in mechanical and robotics engineering from Gwangju Institute of Science and Technology, Gwangju, Republic of Korea. Her current research interest includes prognostics and health management for RCP-VMS.

Minseok Choi received the B.S. degree in mechanical engineering from Gwangju Institute of Science and Technology, Gwangju, Republic of Korea, in 2021, the M.S. degree in mechanical engineering from the Gwangju Institute of Science and Technology, Gwangju, Republic of Korea, in 2022, where he is currently pursuing the Ph.D. degree in mechanical and robotics engineering from Gwangju Institute of Science and Technology, Gwangju, Republic of Korea. His current research interest includes prognostics and health management for RCP-VMS.

Hyunseok Oh received the B.S. degree in mechanical engineering from Korea University, Seoul, South Korea, in 2004, the M.S. degree in mechanical engineering from the Korea Advanced Institute of Science and Technology, Daejeon, South Korea, in 2006, and the Ph.D. degree in mechanical engineering from the University of Maryland, College Park, MD, USA, in 2012. He is an Associate Professor with the department of mechanical and robotics engineering, Gwangju Institute of Science and Technology, Gwangju, Republic of Korea. His research interests include fault diagnostics, industrial artificial intelligence, and model verification and validation.